

# DEM study of the size-induced segregation dynamics of a ternary-size granular mixture in the rolling-regime rotating drum

Shiliang Yang, Liangqi Zhang, Kun Luo, and Jia Wei Chew

Citation: [Physics of Fluids](#) **29**, 123301 (2017);

View online: <https://doi.org/10.1063/1.5008297>

View Table of Contents: <http://aip.scitation.org/toc/phf/29/12>

Published by the [American Institute of Physics](#)

---

## Articles you may be interested in

Numerical study on the axial segregation dynamics of a binary-size granular mixture in a three-dimensional rotating drum

[Physics of Fluids](#) **29**, 103302 (2017); 10.1063/1.5004663

[Collisions of droplets on spherical particles](#)

[Physics of Fluids](#) **29**, 103305 (2017); 10.1063/1.5005124

[Effects of finite-size neutrally buoyant particles on the turbulent flows in a square duct](#)

[Physics of Fluids](#) **29**, 103304 (2017); 10.1063/1.5002663

[Flapping foil power generator performance enhanced with a spring-connected tail](#)

[Physics of Fluids](#) **29**, 123601 (2017); 10.1063/1.4998202

[The mechanism of propulsion of a model microswimmer in a viscoelastic fluid next to a solid boundary](#)

[Physics of Fluids](#) **29**, 121612 (2017); 10.1063/1.4996839

[Autophoretic locomotion in weakly viscoelastic fluids at finite Péclet number](#)

[Physics of Fluids](#) **29**, 123102 (2017); 10.1063/1.5002729

---

**COMPLETELY  
REDESIGNED!**

**PHYSICS  
TODAY**

*Physics Today* Buyer's Guide  
Search with a purpose.

# DEM study of the size-induced segregation dynamics of a ternary-size granular mixture in the rolling-regime rotating drum

Shiliang Yang,<sup>1</sup> Liangqi Zhang,<sup>1</sup> Kun Luo,<sup>2</sup> and Jia Wei Chew<sup>1,3,a)</sup>

<sup>1</sup>School of Chemical and Biomedical Engineering, Nanyang Technological University, Singapore 637459, Singapore

<sup>2</sup>State Key Laboratory of Clean Energy Utilization, Energy Department, Zhejiang University, Hangzhou 310027, People's Republic of China

<sup>3</sup>Singapore Membrane Technology Center, Nanyang Environment and Water Research Institute, Nanyang Technological University, Singapore 637141, Singapore

(Received 5 October 2017; accepted 25 November 2017; published online 14 December 2017)

Segregation induced by size, shape, or density difference of the granular material is inevitable in both natural and industrial processes; unfortunately, the underlying mechanism is still not fully understood. In view of the ubiquitous continuous particle size distributions, this study builds on the considerable knowledge gained so far from binary-size mixtures and extends it to a ternary-size mixture to understand the impact of the presence of a third particle size in the three-dimensional rotating drum operating in the rolling flow regime. The discrete element method is employed. The evolution of segregation, the active-passive interface, and the dynamical response of the particle-scale characteristics of the different particle types in the two regions are investigated. The results reveal that the medium particles are spatially sandwiched in between the large and small particles in both the radial and axial directions and therefore exhibit behaviors intermediate to the other two particle types. Compared to the binary-size mixture, the presence of the medium particles leads to (i) higher purity of small particles in the innermost of the radial core, causing a decrease of the translational velocity of small particles; (ii) decrease and increase of the collision forces exerted on, respectively, the large and small particles in both regions; and (iii) increase in the relative ratio of the active-passive exchange rates of small to large particles. The results obtained in the current study therefore provide valuable insights regarding the size-segregation dynamics of granular mixtures with constituents of different sizes. Published by AIP Publishing. <https://doi.org/10.1063/1.5008297>

## I. INTRODUCTION

Granular material is ubiquitous in the natural and industrial processes. The intrinsic mechanisms governing the granular flow behavior have been rigorously studied at the leading edge of fluid mechanics, solid mechanics, rheology, and statistical physics for centuries.<sup>1–3</sup> As a simple geometrical configuration yet representative of the complex phenomena of granular flow, the rotating drum has been frequently adopted to study the basic mechanisms related to the granular flow from the physical perspective and also practical perspective with respect to the multitudinous industrial applications (e.g., mixing, coating, drying, and chemical reactions in the chemical, pharmaceutical, and metallurgical processes).<sup>1,4–6</sup> As has been analyzed by Mellmann,<sup>7</sup> the flow pattern in the rotating drum can be categorized into six different flow regimes (namely, sliding, avalanching, rolling, cascading, cataracting, and centrifuging) as functions of rotating speed and drum diameter. Furthermore, the difference in the particle properties (e.g., the size, density, and shape) of the granular mixture unavoidably gives rise to radial and axial segregation among the different particle types, which is a complex and

incompletely understood phenomenon without parallel in fluids.<sup>8,9</sup> In most circumstances, the segregation among the granular mixture is undesirable, e.g., radial segregation in the rotating drum could lead to poor contacting efficiency between the gas and small particles in the core and thereby changes the overall bed behavior, while axial segregation may result in products of fluctuating quality.<sup>10</sup> Thus, an in-depth understanding of the segregation phenomenon and the underlying mechanisms in the rotating drum is critical for not only a fundamental understanding but also for the optimal design and operation of this apparatus.

Numerous experimental efforts have focused on studying the granular segregation phenomenon in the rotating drum, with respect to the competition between mixing and segregation,<sup>11</sup> segregation pattern,<sup>12,13</sup> axial transportation,<sup>14</sup> segregation structure,<sup>15</sup> axial segregation and band formation,<sup>16–18</sup> and long-term coarsening.<sup>19</sup> Interesting insights have been obtained, such as, streaks of small particles were observed within regions of large ones whereby the integer number of streaks was fixed over a range of rotation rates;<sup>12</sup> the axial band dynamics was assessed to be driven by global convection throughout the system;<sup>18</sup> and the axial segregation of rotating drum was concluded to have arose from multiple mechanisms.<sup>17</sup> Collectively, the experimental studies have advanced the understanding of granular segregation in the rotating drum.

<sup>a)</sup>Author to whom correspondence should be addressed: JC Chew@ntu.edu.sg.  
Tel.: +65 6316 8916.

However, the opacity of the granular material impedes the experimental quantification of some critical local characteristics of the granular flow (e.g., contacting force and internal segregation structure). To address this, numerical simulation by means of the discrete element method (DEM) has been widely employed due to the ability to track each particle and thereby provide many physical quantities that cannot be easily obtained experimentally.<sup>20–23</sup> As computing speed and capacity progressed, DEM has become an increasingly powerful tool for exploring the mechanisms of dense granular flow.<sup>24,25</sup> Through DEM, Rapaport<sup>26</sup> has numerically modeled a binary-size granular mixture in a three-dimensional (3-D) rotating drum and shown that the results can reproduce the experimental observations of band formation, merging, and motion along the axis. Also based on the DEM simulation, Finnie *et al.*<sup>27</sup> studied the longitudinal and transverse mixing in the rotating drum and concluded that the mixing speed decreases as the rotational speed increases or the fill level increases. Taberlet and Richard<sup>28</sup> found that the axial diffusion characteristics of a binary-size mixture in the rotating drum are such that the axial dispersion of granular flow follows a Gaussian frequency distribution. Rapaport<sup>29</sup> studied the sensitivity of segregation in the rotating drum to the numerical parameters adopted and demonstrated the importance of an appropriate choice of interaction for representing the effective friction force. Chen *et al.*<sup>30</sup> found via DEM that the particle velocity fluctuations are greatest just below the surface and diminish through the depth of the flowing layer. Furthermore, they numerically explored the mechanism that triggers granular axial band formation in the rotating drum and claimed that the axial segregation is initiated by the end wall.<sup>31</sup> Our recent DEM study<sup>32</sup> investigated the segregation of a bi-disperse granular mixture in a 3-D rotating drum operating in the rolling regime and obtained interesting insights like the collision forces exerted on the small and large particles which are, respectively, slightly higher and lower.

Although reports regarding granular segregation are not lacking, most of them are focused on the segregation dynamics of the binary-size mixture, despite the granular mixtures being typical of polydisperse size distributions in nature and in practical industrial processes. In the practical operation, it is meaningful to explore the flow behavior of granular material with more particle sizes than the more understood binary mixtures, as the realistic material always shows considerable size ranges.<sup>33</sup> Moreover, as highlighted by Newey and Ozik,<sup>34</sup> the number of particle sizes in a mixture is a useful variable for investigating the granular segregation and also is valuable for evaluating the predictive power of the segregation models that have been developed for monodisperse and binary-size systems. Granular flow behaviors of ternary mixtures have been reported in granular systems besides the rotating drum, and the corresponding interesting phenomena have been obtained, for example, in heap formation whereby alternative layers of different particle sizes were observed,<sup>35</sup> sandpile whereby the importance of the ratios of the different grain types on pattern formation was underscored,<sup>36</sup> and hopper<sup>33</sup> and vibrated systems<sup>37</sup> whereby the effect of a third granular material on the discharge was reported. Exploring the effect of an additional granular type in the more widely reported binary

mixtures is an important step towards more closely mimicking the prevalent continuous particle size distributions and is critical from both the perspectives of fundamental understanding and practical operations. The related studies on the segregation dynamics of multiple-size granular mixtures in the rotating drum are comparatively limited relative to that of binary mixtures, and only the following experimental and numerical ones are available in the literature. Das Gupta *et al.*<sup>10</sup> experimentally found that the axial segregation of a ternary mixture is similar to that of a binary mixture in that radial segregation appeared before axial segregation. Newey and Ozik<sup>34</sup> demonstrated experimentally that the bands in ternary mixtures oscillate axially under some conditions. Furthermore, Hajra and Khakhar<sup>38</sup> experimentally observed that the driving forces causing the radial segregation of ternary mixtures consisting of particles differing in size and density segregate may complement or oppose each other. Using DEM, Rapaport<sup>39</sup> reported that the band formation is such that the medium-size particles tend to be located between alternating bands of the large and small particles. Pereira and Cleary<sup>40</sup> subsequently showed numerically that the extent of segregation of a ternary mixture is much reduced compared to the equivalent binary system. Recently, Alizadeh *et al.*<sup>41,42</sup> experimentally and numerically explored the mixing and segregation of granular flow of a mixture with four particle sizes in the rotating drum and indicated that the medium-size particles are found throughout the drum. The experimental work of Tilo<sup>19</sup> demonstrated that (i) the stripe stability due to granular segregation can be controlled by the addition of a few percent of different-sized grains and (ii) the bands of monodisperse small grains do not show merging or coarsening, which raises the importance of further studying the mechanism and the effect of adding another granular material to the bi-disperse granular mixture. The experimental work of Hajra and Khakhar<sup>38</sup> illustrated that in a few of the mixtures, the behavior of the system is more complicated than that expected from pairwise interactions due to the presence of the third component. Collectively, although some understanding on the effect of multiple sizes in the rotating drum has been obtained, a gap in the knowledge base still exists regarding the fundamental aspects [e.g., the velocity, force, and solid residence time (SRT)] of the different particle types, the role of the third granular type, and the related dynamical response to the radial and axial segregation phenomena.

Accordingly, to further understand the segregation dynamics of multi-component mixtures, the current study is targeted at exploring the segregation dynamics by means of DEM of the dense granular flow of a ternary-size mixture in the three-dimensional (3-D) rotating drum operating in the rolling flow regime, which is the typical operating mode in industrial processes.<sup>42</sup> At first, the general segregation trend within the system is studied, followed by the identification of the active-passive interface. Then, the dynamical response to the segregation phenomenon, the axial distribution characteristics, and the comparison between the active and passive regions of the particle-scale quantities (i.e., the velocity and collision force) of different particle types are discussed. After that, the distribution of solid residence time in both the active and passive regions and the exchanging intensity between the

two regions are assessed. Finally, the spatially resolved distributions of the axial dispersion in the transverse plane and axially are studied.

## II. COMPUTATIONAL METHODS

In the current study, DEM is employed to resolve the granular behavior at the particle-scale level, that is, every particle is tracked in the Lagrangian framework. Each particle interacts with the neighboring particles, drum wall and the fluid. In view of the gas density being three orders-of-magnitude smaller and the gas motion being relatively negligible, the force exerted by the gas phase is negligible and thus the force exerted on a specific particle consists of the gravity, the collision force due to the neighboring particles and wall. In the Lagrangian framework, the motion of a particle is governed by Newton's second law, and the corresponding governing equations for the translational and rotational motion of this particle can be described as

$$m_i \frac{d\mathbf{v}_i}{dt} = \sum_{j=1}^k \mathbf{F}_{c,ij} + m_i \mathbf{g}, \quad (1)$$

$$I_i \frac{d\omega_i}{dt} = \sum_{j=1}^k \mathbf{M}_{ij}, \quad (2)$$

where  $m_i$  and  $I_i$  are, respectively, the mass and moment of inertia of this particle;  $\mathbf{v}_i$  and  $\omega_i$  stand for, respectively, the translational and rotating velocities of particle  $i$ ;  $\mathbf{g}$ ,  $k$ , and  $t$  represent, respectively, the gravitational acceleration, the total number of particles and wall colliding with the current particle, and time instant;  $\mathbf{F}_{c,ij}$  and  $\mathbf{M}_{ij}$  stand for, respectively, the collision force and torque generated between the colliding pair of particle  $i$  and particle  $j$ .

In the rotating drum, the dense flow behavior of the solid phase gives rise to intensive collisions between the neighboring particles. Thus, treating the collision behavior between particles is critical for accurately capturing such collision-dominated flow in the rotating drum. To achieve this, the soft-sphere collision model initially proposed by Cundall and Strack<sup>43</sup> is adopted since it treats multiple collisions concurrently. In this model, the contacting process of neighboring particles is achieved by using the combination of the spring, dashpot, and slider to consider the overlap between them. Between a colliding pair, the collision force ( $\mathbf{F}_{c,ij}$ ) has a strong relationship with the overlap displacement ( $\delta$ ) due to the deformation of colliding pair and the relative colliding velocity ( $\mathbf{v}_{n,ij}$ ), and it can be divided into the tangential ( $\mathbf{F}_{ct,ij}$ ) and normal ( $\mathbf{F}_{cn,ij}$ ) components along the tangential

and normal directions of the colliding pair. The equations for evaluating the collision forces between collision pair can be described as

$$\mathbf{F}_{c,ij} = \mathbf{F}_{cn,ij} + \mathbf{F}_{ct,ij}, \quad (3)$$

$$\mathbf{F}_{cn,ij} = k_{n,ij} \delta_{n,ij} \mathbf{n} + \gamma_{n,ij} \mathbf{v}_{n,ij}, \quad (4)$$

$$\mathbf{F}_{ct,ij} = \min \left\{ \left( k_{t,ij} \delta_{t,ij} \mathbf{t} + \gamma_{t,ij} \mathbf{v}_{t,ij} \right), \mu \mathbf{F}_{cn,ij} \right\}, \quad (5)$$

where the  $n$ ,  $t$ ,  $\mathbf{n}$ , and  $\mathbf{t}$  stand for, respectively, the normal component of a variable, the tangential component of a variable, the normal unit vector, and the tangential unit vector;  $\mu$  is the friction coefficient adopted to evaluate the tangential collision force when slide occurs between colliding particles. The stiffness coefficient ( $k$ ) and the damping coefficient ( $\gamma$ ) are related to the material property (i.e., Young's modulus, the Poisson ratio, and the restitution coefficient) and the related calculation details can be found in Table I. Note that rolling friction is included in some DEM models to account for various rolling resistance effects (e.g., viscous hysteresis, surface adhesion, and shape effects),<sup>44–46</sup> but not in this study since the lack of it still gave good agreement between the model and experimental results in terms of various characteristics assessed (e.g., depth of active region, dynamic angle of repose, and streamwise velocity distribution).<sup>47</sup>

## III. NUMERICAL SETUP AND MODEL VALIDATION

### A. Numerical setup

The rotating drum studied in the current work is a 3-D horizontal cylinder rotating around its central axis. It has a diameter of 0.24 m in the transverse ( $x$ - $y$ ) plane and a length of 0.72 m in the axial ( $z$ ) direction. The Cartesian coordinates are adopted with the origin in the geometrical center of the system, the  $y$ -direction opposite to the direction of gravity, the  $z$ -direction along the drum length, and the  $x$ -direction perpendicular to both the  $y$ - and  $z$ -direction.

Figure 1 presents a 3-D illustration of the geometrical configuration and the instantaneous distribution of the particles in the rotating drum at the time instant of 260 s. The particles are glass spheres with a density of 2500 kg/m<sup>3</sup>. A total number of 235 121 particles are used to fill the rotating drum to a volumetric fill level of 35%. Specifically, the rotating drum contains a ternary-size mixture, made up of particles with three different diameters, namely, 6 mm (large), 4.5 mm (medium), and 3 mm (small), at a mass ratio of 1:1:1; the corresponding number of particles are 20 676, 49 015, and 165 430, respectively.

TABLE I. Details of the equations adopted to calculate the collision force in the soft-sphere collision model.

Normal and tangential stiffness coefficients $k_{n,ij}$ and $k_{t,ij}$
$k_{n,ij} = \frac{4}{3} Y^* \sqrt{R^* \delta_{n,ij}}$ , $k_{t,ij} = 8G^* \sqrt{R^* \delta_{n,ij}}$
Normal and tangential damping coefficients $\gamma_{n,ij}$ and $\gamma_{t,ij}$
$\gamma_{n,ij} = 2\sqrt{\frac{5}{6}} \beta \sqrt{S_{n,ij} m^*}$ , $\gamma_{t,ij} = 2\sqrt{\frac{5}{6}} \beta \sqrt{S_{t,ij} m^*}$
where the variables with asterisk stand for the reduced parameters and the corresponding variables are evaluated as:
$\beta = \frac{\ln(e)}{\sqrt{\ln^2(e) + \pi^2}} S_{n,ij} = 2Y^* \sqrt{R^* \delta_{n,ij}}$ , $S_{t,ij} = 8G^* \sqrt{R^* \delta_{n,ij}}$ , $\frac{1}{Y^*} = \frac{(1-\nu_i^2)}{Y_i} + \frac{(1-\nu_j^2)}{Y_j}$ , $\frac{1}{R^*} = \frac{1}{R_i} + \frac{1}{R_j}$ , $\frac{1}{m^*} = \frac{1}{m_i} + \frac{1}{m_j}$ ,
$\frac{1}{G^*} = \frac{2(2+\nu_i)(1-\nu_i)}{Y_i} - \frac{2(2+\nu_j)(1-\nu_j)}{Y_j}$

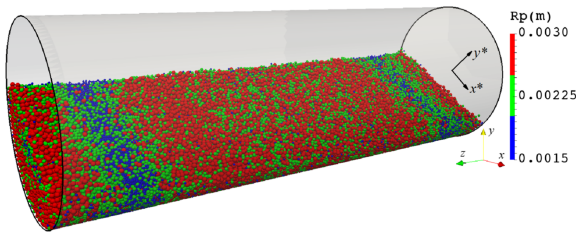


FIG. 1. Snapshot of the instantaneous particle distribution in the three-dimensional (3-D) rotating drum at the time instant of 260 s.

Initially, all the particles are generated in the whole drum and then allowed to fall freely by gravity to form a packed bed when the total kinetic energy decays to zero. After this, the drum starts to rotate at a speed of 11.6 rpm, which corresponds to a Froude number<sup>8</sup> of 0.000 457 and thus operates in the rolling regime. Details related to the particle properties and numerical parameters adopted are listed in Table II.

To track the velocity and position of the particles, the governing equations of motion are discretized and then integrated with a time step of  $1.0 \times 10^{-6}$  s in the current study. Due to the small time step adopted and a large number of particles tracked, the whole system runs in the parallel mode with a total number of 32 CPUs. A total duration of 280 physical seconds is simulated.

## B. Model validation

Proper validation of the numerical simulation is extremely vital for the reliability of the numerical results and the related discussions. For the current study, the numerical validation has been carried out based on the experimental study on monodisperse particles in a rotating drum with the same dimensions.<sup>41</sup> Several aspects related to the rotating drum operating in the rolling regime have been evaluated and compared with the experimental data, including the (i) the dynamic angle of repose for the solid flow in the central and near-wall slice, (ii) the active region thickness, and (iii) the time-averaged velocity of particles parallel and perpendicular to the bed surface. The numerical results of these aspects agree well quantitatively with the experimental data of Alizadeh *et al.*,<sup>41</sup> demonstrating the proper implementation and selection of the

TABLE II. Details of the physical and numerical parameters adopted.

Drum properties	
Drum diameter (m)	0.24
Drum axial length (m)	0.72
Rotating speed (rpm)	11.6
Particle properties	
Particle density ( $\text{kg}/\text{m}^3$ )	2500
Particle diameter (mm)	6.0, 4.5, and 3.0
Young's modulus (Pa)	$1.0 \times 10^8$
Poisson ratio (...)	0.24
Restitution coefficient of particle-particle collision (...)	0.97
Restitution coefficient of particle-wall collision (...)	0.85
Friction coefficient of particle-particle collision (...)	0.30
Friction coefficient of particle-wall collision (...)	0.35

numerical parameters for the current system. Details related to the model validation can be found in our previous work.<sup>47</sup> In contrast to the previous study on a monodisperse particle system, this study focuses on (i) a ternary-size mixture with the same material property and (ii) an extended drum length that is twice that of the previous.<sup>47</sup>

## IV. RESULTS AND DISCUSSION

To understand the segregation dynamics of the ternary-size mixture in the rotating drum, several aspects of the particle motion are presented here. First, the segregation behavior of the mixture is qualitatively described via the instantaneous distribution of particles at several time instants, and the active-passive interface is identified. Then, the segregation phenomenon is evaluated through the particle velocity, collision force, and trajectory of each particle type. After that for each particle type, the solid residence time (SRT) in each region, the exchange rate of the particles between the active and passive regions, and the axial dispersion tendencies are assessed.

### A. Dynamical segregation behavior

Figure 2 illustrates the instantaneous distribution of the particles in the central ( $z/Z = 0$ , where  $z$  is the axial position evaluated and  $Z$  is the half-drum length of 0.36 m) and near-wall ( $z/Z \sim 1$ )  $x$ - $y$  slices of the rotating drum containing the ternary-size mixture at several different time instants. The general flow characteristics and the dynamical segregation behavior of the ternary-size granular mixture can be summarized as follows. Initially at  $t = 10$  s [Figs. 2(a) and 2(f)], radial segregation is apparent, specifically in that the small particles tend to dominate in the radial center at both axial positions, with such radial segregation relatively more extensive near the wall [Fig. 2(f)]. At  $t = 40$  s [Figs. 2(b) and 2(g)], radial segregation is more extensive and axial segregation becomes clear. The radial segregation is such that the radial core is almost wholly composed of small particles at both axial positions, while the radial demarcation between the medium and large particles is less distinct though slightly more extensive at the central slice. As for axial segregation, it is clear that the proportion of large particles is lower at the central slice [Fig. 2(b)] and predominant at the near-wall slice [Fig. 2(g)]. At  $t = 140$  s [Figs. 2(c) and 2(h)], the segregation patterns appear to have stabilized and remain similar beyond this time point [Figs. 2(d), 2(e), 2(i), and 2(j)]. At the central slice [ $z/Z = 0$ ; Figs. 2(c)-2(e)], the radial center of the bed is made up almost completely of small particles, followed by an outer ring made up more dominantly of the medium particles, and then the periphery consists mainly of large particles. At the near-wall slice [ $z/Z \sim 1$ ; Figs. 2(h)-2(j)], the large particles clearly dominate, although a radial center with a higher proportion of the medium particles is visible. In general, the immediate appearance of the radial segregation is mainly due to the void-filling percolation, i.e., the random fluctuations within the flowing avalanche in the active region open up inter-particle gaps and small particles more likely fall into the gaps under the effect of gravity.<sup>48</sup> The intrinsic mechanism underlying the slow axial segregation is a long-existing puzzle to the physics community that is

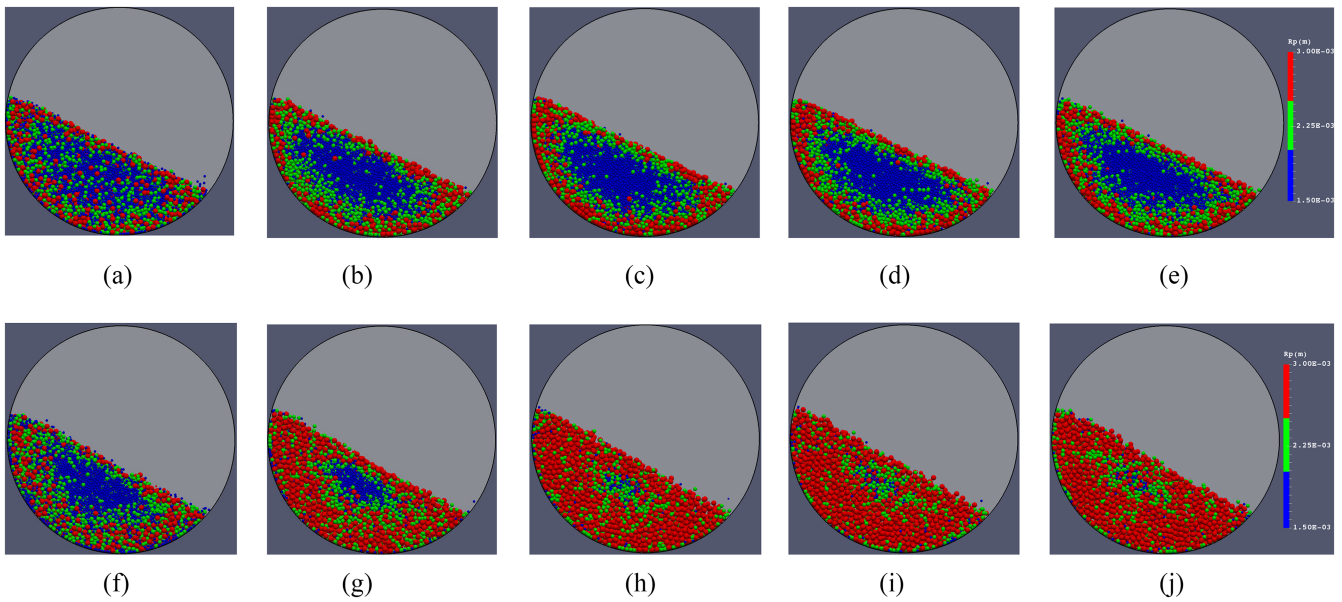


FIG. 2. Dynamical segregation behavior of the ternary-size mixture (the large, medium, and small particles are red, green, and blue, respectively) in the central and near-wall ( $x$ - $y$ ) slices of the drum at several time instants. [(a)-(e)]: Central slice ( $z/Z = 0$ ) and [(f)-(j)]: near-wall slice ( $z/Z \sim 1$ ). (a)  $t = 10$  s, (b)  $t = 40$  s, (c)  $t = 140$  s, (d)  $t = 200$  s, (e)  $t = 260$  s, (f)  $t = 10$  s, (g)  $t = 40$  s, (h)  $t = 140$  s, (i)  $t = 200$  s, and (j)  $t = 260$  s.

not fully resolved. Over the past decades, several mechanisms have been proposed to elucidate the onset of this phenomenon, but none can yet provide a complete and universally applicable explanation. For example, Hill and Kakalios<sup>49</sup> claimed that the difference in the angle of repose of different particle types results in axial segregation. By numerically comparing drums with a wall or periodic boundary condition, Chen *et al.*<sup>31</sup> proposed that the end walls initiate the axial segregation via an axial flow due to friction at the end walls,<sup>31</sup> after which the non-uniform distribution of axial flow velocity combined with radial segregation due to percolation leads to the small particles being driven further from the end walls and the accumulation of large particles near the end walls.<sup>31</sup> The faster radial segregation and slower wall-induced axial segregation, as well as the preferential radial segregation of the small particles to the radial center and the axial segregation of the large particles to the wall, agree with previous studies.<sup>32,39</sup> Furthermore, this observed phenomena confirm the previous findings from the studies of Hajra and Khakhar,<sup>38</sup> Rapaport,<sup>39</sup> and Pereira and Cleary<sup>40</sup> that the notable characteristic for the ternary-size mixture, as compared with the binary-size mixture,<sup>32</sup> is that the medium particles tend to be in between the small and large ones and the more obvious segregation of small particles located in the innermost of the core and of large particles in the near-wall region.

To illustrate the overall segregation behavior in the rotating drum, Fig. 3 presents the 3-D representation of the ternary-size mixture in terms of iso-surfaces denoting positions at which the mass fractions of each species are 0.5. Specifically, the red, green, and blue iso-surfaces represent positions at which the mass fractions of, respectively, the large, medium, and small particles are 0.5 at the time instant of 260 s, which corresponds to the instantaneous particle distribution in Fig. 1. The size-segregation is clear. Radially, the small particles are in the center and the large particles are in the

periphery, while the medium ones are in between. Axially, the axial bands consisting almost completely of a single type of particles are clear, in terms of two axial bands of large particles at the end walls, followed by two adjacent narrower axial bands of medium particles, and then by two axial bands of small particles. Collectively, Figs. 2 and 3 indicate that the medium particles are generally in between the small and large particles, both radially and axially throughout the whole drum.

### B. Active-passive interface

In the rolling regime studied here, it is well known that the rotating drum has two distinct regions, namely, the active and passive regions, with significantly different granular flow behaviors. Therefore, it is meaningful to geometrically separate these two regions to better analyze the flow characteristics of the different particle types of the ternary-size granular mixture. Similar to the criterion adopted by previous reports,<sup>41,42,50</sup> the active-passive interface is identified as the positions at which the streamwise velocity of the particles equal zero

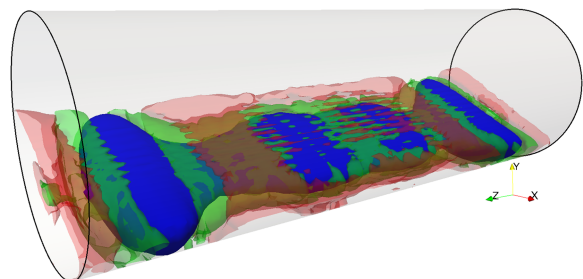


FIG. 3. 3-D illustration of the segregation structure of the ternary-size granular mixture in the rotating drum at the time instant of 260 s, whereby red, green, and blue iso-surfaces represent positions at which the mass fractions of, respectively, the large, medium, and small particles are 0.5.

(i.e., the streamwise velocity transition between positive and negative). Specifically, the streamwise velocity is that parallel to the particle bed surface, and thus another coordinate system  $x^*$ - $y^*$  (Fig. 1) is adopted with the  $x^*$  and  $y^*$  axes being, respectively, parallel and perpendicular to the bed surface. In the current work, since the particles are tracked individually in the Lagrangian framework, the mapping from the Lagrangian framework to the Eulerian framework is achieved based on each particle center. Similar to our previous work,<sup>47</sup> this protocol is such that the rotating drum is first enclosed with a cube with dimensions of 0.24 m, 0.24 m, and 0.72 m along the  $x$ ,  $y$ , and  $z$  directions, respectively, after which the cube is divided into smaller grid cells with dimensions of 3 mm, 3 mm, and 12 mm along the  $x$ ,  $y$ , and  $z$  directions, respectively. Subsequently, the instantaneous particle velocity in a local grid cell  $i$  is evaluated as the mass-weighted average of the instant velocities of all the particles ( $N_p$ ) located in this cell at the time instant evaluated by

$$U_{i,t} = \frac{\sum_{j=1}^{N_p} m_j v_{i,j}}{\sum_{j=1}^{N_p} m_j} \quad (i = x, y, z), \quad (6)$$

where  $v_{i,j}$  and  $m_j$  are, respectively, the instantaneous velocity and mass of the particle  $i$ . Finally, the time-averaged streamwise velocity of particles based on the local  $x^*$ - $y^*$  coordinate system is obtained by transcribing the particle velocity from the  $x$ - $y$ - $z$  coordinate system and then time-averaging over all the  $N_t$  samples,

$$U_{sx^*} = \frac{\sum_{t=1}^{N_t} (U_{x,i} \cdot \cos(\theta) - U_{y,i} \cdot \sin(\theta))}{N_t}, \quad (7)$$

where  $\theta$  is the dynamic angle of repose evaluated as the slope of the bed surface.

Based on the above-mentioned approach, Fig. 4(a) presents the time-averaged streamwise velocity of the solid phase in the central  $x$ - $y$  slice of  $z/Z = 0$ . In general, the active region is the upper part of the rotating drum where the particles cascade downwards, and the comparatively less vigorous passive region is the lower part where the particles are carried upwards by the drum wall. Similar to the trends for monodisperse<sup>47</sup> and binary mixtures,<sup>32</sup> Fig. 4(a) shows that the particles generally follow semi-circular trajectories, with the streamwise velocities near the bed surface being significantly higher due to rapidly falling behavior in the avalanche and opposite in direction from that lower in the bed. Because of the change in

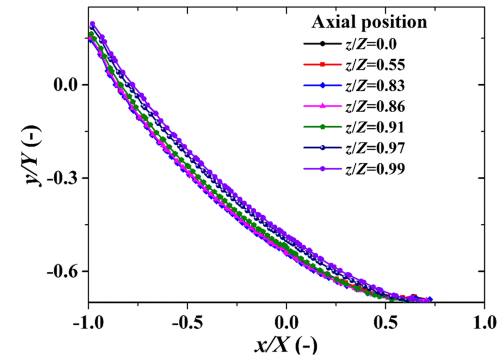


FIG. 5. Comparison of the active-passive interfaces along the axial length of the rotating drum.

the direction of the particles as they fall along the bed surface and approach the wall, the streamwise velocity (i.e., velocity parallel to the bed surface) changes from positive to negative. Thus, the 3-D active-passive interface identified by the positions at which the streamwise velocities are zero (i.e., transitions between positive and negative) is illustrated in Fig. 4(b). It is evident that the active-passive interface is a smooth surface across the entire axial drum length and becomes more concave near the end walls.

Figure 5 further quantitatively compares the height of the active-passive interface along the drum length to evaluate the impact of the end walls. The curvatures of the interfaces are similar. Notably, while the heights of the interfaces are similar throughout approximately 80% of the axial length of the drum (i.e.,  $|z/Z| \leq 0.91$ ), those nearer the end walls (i.e.,  $|z/Z| > 0.91$ ) become higher, reflecting the non-negligible influence of the end walls on the active-passive interface, which is similar to that in the monodisperse<sup>47</sup> and binary-size mixture.<sup>32</sup>

### C. Velocity distribution

In contrast to the monodisperse system, the size-segregation phenomenon inherent in polydisperse mixtures changes the distribution of the different particle types in both the transverse and axial directions, which would affect the distributions of the velocities of the different particle types. Figure 6(a) presents the evolution of the instantaneous velocities (obtained by averaging over the whole drum) in all three directions for each of the three particle types, while Fig. 6(b) presents the time-averaged velocities with respect to the axial

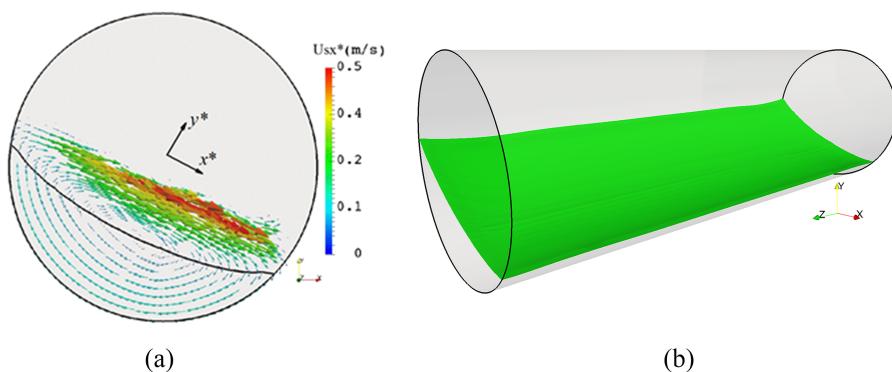


FIG. 4. (a) Vectors of the time-averaged streamwise velocity ( $U_{sx^*}$ ) of the particles in the central  $x$ - $y$  slice of  $z/Z = 0$ , and (b) 3-D illustration of the active-passive interface identified by the positions at which the streamwise velocity ( $U_{sx^*}$ ) in the rotating drum is zero.

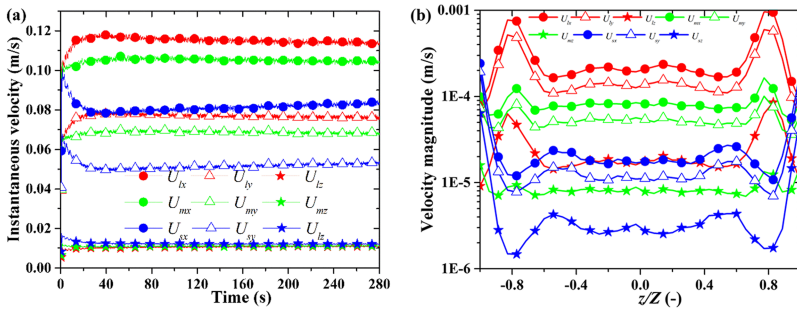


FIG. 6. Velocity profiles in all three directions of each particle type in the rotating drum: (a) evolution with time of the instantaneous velocity of each particle type averaged over the whole rotating drum and (b) time-averaged velocities with respect to axial position.

position along the drum length (axially divided into 36 sections). Specifically, the profiles plotted with red, green, and blue colors represent, respectively, for the velocities of the large, medium, and small particle type, while the circle, triangle, and star symbols stand, respectively, for the  $x$ ,  $y$ , and  $z$  components.

Three observations are clear in Fig. 6(a). First, the radial segregation phenomenon at  $t < 40$  s gives rise to the sharp increase and decrease in the velocities, respectively, of the large and small particles, whereas relatively negligible changes in that of the medium particles. The greater changes of the large and small particles are because of the radial segregation, respectively, to the periphery and inner core, which thereby causes the large particles to be in the faster-moving active region and the small particles to be in the slower-moving passive region. As for the medium particles because they tend to be sandwiched between the large and small particles (Figs. 2 and 3), they are scattered in both active and passive regions, and correspondingly the change in their velocities is lesser. Second, the change in velocities for all three particle types are relatively lesser at  $t > 40$  s due to the relatively negligible radial segregation. However, in contrast to  $t < 40$  s, the velocities of the large and small particles exhibit, respectively, decreasing and increasing velocities. On the other hand, similar to  $t < 40$  s, the change of velocities of the medium particles is relatively lesser than that of the large and small ones. Third, for all three particle types, the velocity component along the  $x$  direction is the greatest due to the drum rotation, followed by the velocity component along the  $y$  direction due to gravity, and lastly the velocity component along the  $z$  direction which is tied to end-wall effects and the slow axial segregation. Therefore, Fig. 6(a) indicates clearly that the radial and axial segregation exerts limited influences on the velocities of the medium particles.

As described above (Figs. 2 and 3), the axial segregation along the drum length leads to the re-distribution of different particle types and also the formation of bands dominated by a specific particle type, which would influence the velocity magnitude of different particle types along the axial ( $z$ ) direction. To study this, the time-averaged (i.e., between  $t = 4$ – $280$  s) velocity of each particle type in all three directions is quantified in each of the 36 sections along the drum length, as displayed in Fig. 6(b). Five observations are noted. First, the axial velocity distributions of all three directional components of all three particle types are non-uniform, with the flattest profiles exhibited by the medium particles. Second, radial segregation gives rise to the greatest velocity

magnitudes for the large particles along the transverse plane (i.e.,  $x$  and  $y$ ), followed by the medium particles and then the small particles. Third, the formation of the bands of small particles near the end walls ( $z/Z = \pm 0.8$ ) leads to enhanced velocities of the large and medium particles, since the dominance of the small particles severely reduces the particle number of these two particle types, which tend to be more extensively radially segregated to the periphery and therefore active region. Fourth, the formation of the bands of large particles at the end walls ( $z/Z \sim \pm 1$ ) severely diminishes the velocities of the large particles due to the accumulation of the large particles in the slower-moving inner core. Fifth, the nearly generated bands of small particles near  $z/Z = \pm 0.6$  give rise to larger velocity components of the small particles as they start to accumulate in the radial periphery. In view of the two regions (i.e., active and passive) with distinctive flow behaviors, further assessment of the velocities is carried out to understand the characteristics of a ternary-size granular mixture. The velocity component of each particle type in these two regions, based on the active-passive interface detected above (Fig. 5), can be obtained by evaluating the instantaneous mean velocity of all the particles of a specific particle type. The obtained means of all three velocity (both translational and rotating) components of all three particle types in the active and passive regions are listed in Table III. In general, the rapid flow in the active region and the relatively slower-moving passive region gives rise to the following: (i) whereas the translational velocities in the transverse plane (i.e.,  $U_x$  and  $U_y$ ) are up to an order-of-magnitude greater than that in the axial direction (i.e.,  $U_z$ ), the rotational velocities in the transverse plane (i.e.,  $\omega_x$  and  $\omega_y$ ) are lower than that in the axial direction (i.e.,  $\omega_z$ ); (ii) in the transverse plane (i.e.,  $x$  and  $y$  directions), the translational velocities (i.e.,  $U_x$  and  $U_y$ ) in the active region are approximately two times of the corresponding ones in the passive region, while the rotating velocities (i.e.,  $\omega_x$  and  $\omega_y$ ) in the active region are three to four times of that in the passive; (iii) the transverse translational velocities (i.e.,  $U_x$  and  $U_y$ ) increase with particle diameter in both the active and passive regions, while the axial translational velocity ( $U_z$ ) increases with particle diameter in the active region but decreases with particle size in the passive region; and (iv) the rotational velocities in all three directions ( $\omega_x$ ,  $\omega_y$ , and  $\omega_z$ ) decrease with particle diameter in both the active and passive regions due to the decrease of moment of inertia. All these observations for the ternary-size mixture are similar to that for the binary-size mixture.<sup>32</sup> Quantitatively comparing the

TABLE III. The time-averaged translational and rotating velocities of the three particle types in the active and passive regions of the rotating drum.

	$U_x$ (m/s)	$U_y$ (m/s)	$U_z$ (m/s)	$\omega_x$ (deg/s)	$\omega_y$ (deg/s)	$\omega_z$ (deg/s)
Large particles in active region	0.205	0.108	0.027	9.9	9.13	13.4
Medium particles in active region	0.178	0.096	0.026	12.78	12.4	16.45
Small particles in active region	0.12	0.07	0.024	18.2	18.7	22.23
Large particles in passive region	0.084	0.066	0.0049	2.21	2.3	3.4
Medium particles in passive region	0.078	0.059	0.0055	3.3	3.5	4.5
Small particles in passive region	0.064	0.045	0.0073	6.6	7.1	7.9

flow characteristics of the large and small particles with that in the binary-size system, the presence of the medium particle type has the following effects on the translational and rotational velocities: (i) it exerts negligible influence on the velocities of the large particles along all three directions in both the passive and active regions, which is mainly because the large particles persist in preferentially segregating to the periphery; (ii) it decreases the  $x$ - and  $y$ -directional translational velocities ( $U_x$  and  $U_y$ ) of small particles by approximately 10% in both the active and passive regions, which is mainly because the small particles are more concentrated towards the inner core, and thus exhibit a smaller velocity in the transverse plane [Fig. 4(a)]; and (iii) the axial velocities ( $U_z$ ) of both the large and small particles are similar in both the ternary-size and binary-size mixtures, indicating that the presence of the third particle type does not change the random collisional motion of both the large and small particles.

#### D. Collision level information

In the rotating drum, the frequent collisions between neighboring particles and the corresponding collision-dominated flow characteristics need to be understood for each particle type. The motion of the particles especially in the axial direction is strongly influenced by the collision between particles, and thus a closer assessment of the collisions may provide some insights into the complex phenomena like axial segregation and band travelling. Figure 7 presents the contour plot of the spatially resolved distribution of the mass-averaged collision force between colliding particles in the central slice  $z/Z = 0$  of the rotating drum, with each black line representing the active-passive boundary in each slice. Three observations are worth noting. First, the collision forces in all three directions in the active region are obviously larger than that in the passive region due to the more rapid flow. Second, the force distributions are different in the three directions.

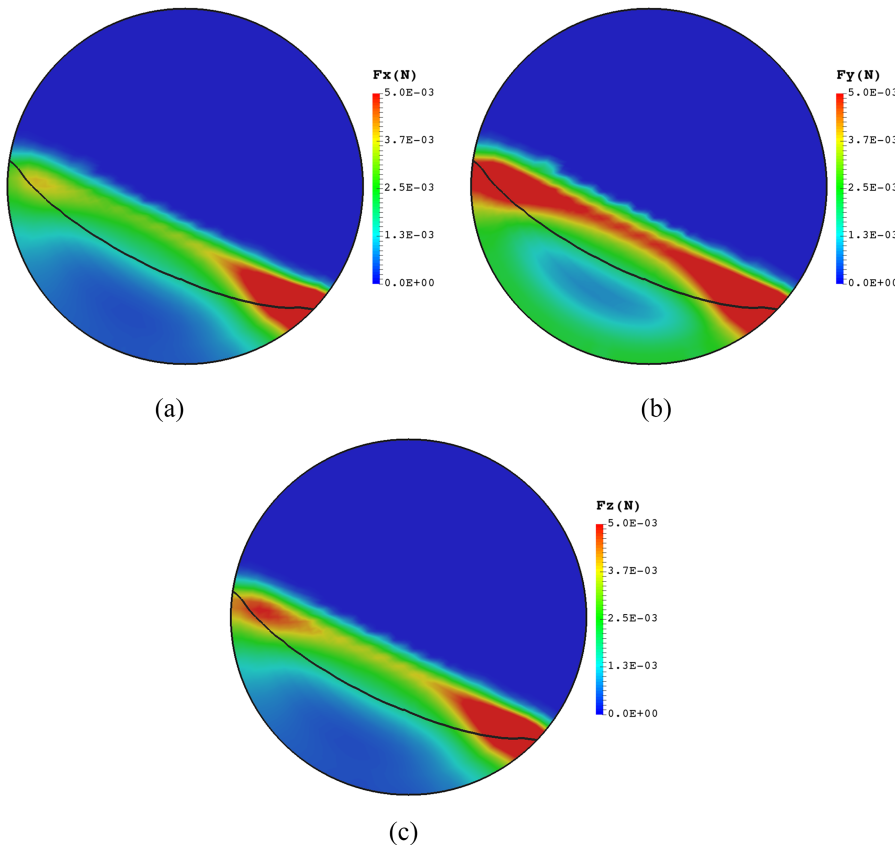


FIG. 7. Contour plot of the spatially resolved distribution of the mass-averaged collision force exerted on the colliding particles in the central slice  $z/Z = 0$  of the rotating drum, where each black line stands for the active-passive boundary: (a)  $F_x$ ; (b)  $F_y$ ; (c)  $F_z$ .

For the  $x$ -component collision force [ $F_x$ ; Fig. 7(a)], the greatest  $F_x$  magnitudes lie at the lower end of the active region due to the intensive collisions of the falling particles. For the  $y$ -component collision force [ $F_y$ ; Fig. 7(b)], the least  $F_y$  magnitudes are in the radial core, while the greatest are near the particle bed surface of the active region due to the intensive collision induced by the falling particles. As for the  $z$ -component collision force [ $F_z$ ; Fig. 7(c)], the greatest  $F_z$  magnitudes are at the two ends of the active region induced by collisions with the drum wall. Third, compared to  $F_x$  and  $F_z$ , the  $F_y$  magnitudes are generally greater in the passive region, particularly near the bottom wall, due to the gravitational force effects. Qualitatively comparing the collision force distribution of the ternary-size mixture with the binary-size granular mixture<sup>32</sup> demonstrates that the presence of the third particle type does not change the general distributions of this force in the rotating drum.

To quantitatively compare the different flow characteristics of each particle type induced by the size-segregation effect, the evaluation of the collision force exerted on each particle type is conducted by first non-dimensionalizing the collision force with respect to the gravitational force. Figure 8(a) presents the evolution of the non-dimensionalized collision forces exerted on all three particle types along all three directions. The trends are noted as follows: (i) the non-dimensionalized forces exerted on the small particles are the greatest along all three directions, followed by the medium particles and then the large particles; (ii) for the three force components, the  $y$ -component is the largest, while the  $x$ - and  $z$ -components are more similar; (iii) radial segregation within the initial time period of 40 s gives rise to steeper changes with time of the collision forces, especially the large and small ones, while axial segregation leads to more gradual changes with time.

To evaluate the effect of axial segregation on the collision forces, Fig. 8(b) presents the axial distribution of the non-dimensionalized collision force exerted on the different particle types. Specifically, the whole drum length was divided into 36 uniform slices, and then the non-dimensionalized collision forces are time-averaged within each slice. It is observed that (i) across the whole drum length, the relative magnitudes of the forces are the same as that in Fig. 8(a), and (ii) the formation of the axial bands leads to non-uniform distributions of the collision forces with peaks and valleys corresponding to the axial bands of large and small particles, respectively.

The non-dimensionalized force of each particle type in the two distinct regions of the rotating drum (i.e., active and

TABLE IV. The time-averaged non-dimensionalized collision force exerted on the three particle types in the active and passive regions of the rotating drum.

	$F_x/G_p$ (-)	$F_y/G_p$ (-)	$F_z/G_p$ (-)
Large particles in active region	1.84	2.65	1.97
Medium particles in active region	2.15	3.03	2.34
Small particles in active region	5.29	7.07	5.77
Large particles in passive region	0.88	1.6	0.89
Medium particles in passive region	0.83	1.32	0.87
Small particles in passive region	2.17	2.82	2.28

passive) is analyzed by averaging all the variables exerted on the particles in the corresponding regions over the entire simulation time. Table IV lists the values which indicate that (i) along all three directions and in both regions, the collision force exerted on the small particles is two to three times that on the large or medium particles, (ii) for all three particle types, the collision force in the active region is about two times of that in the passive region, and (iii) in both the active and passive regions, for all three particle types, the  $y$ -component collision force is the greatest, followed by the  $z$ -component and then the  $x$ -component. Quantitatively comparing these with the binary-size mixture<sup>32</sup> reveals that the presence of the medium particles decreases and increases the collision force exerted, respectively, on the large and small particles in both the active and passive regions.

## E. Typical trajectory of the three particle types

To gain more insights on the radial segregation, Fig. 9 illustrates the typical trajectories of the three particle types over the entire simulation duration. In general, the radial segregation of the ternary-size granular mixture is such that the small particles progressively congregate in the radial core, the large ones in the radial periphery, and the medium ones sandwiched in between the other two. More importantly, presenting the trajectories of the three particle types provides a direct and vivid illustration regarding the residence time behavior, the circulation, and also the exchanging tendencies between the active and passive regions. In view of the different flow behaviors, it is meaningful to evaluate these essential characteristics in the two distinct regions of the rotating drum. For instance, the rate of exchange of each particle type across the active-passive interface can be tracked to provide insights regarding the tendency of the particles to traverse the two regions. Since every particle in the rotating drum is tracked

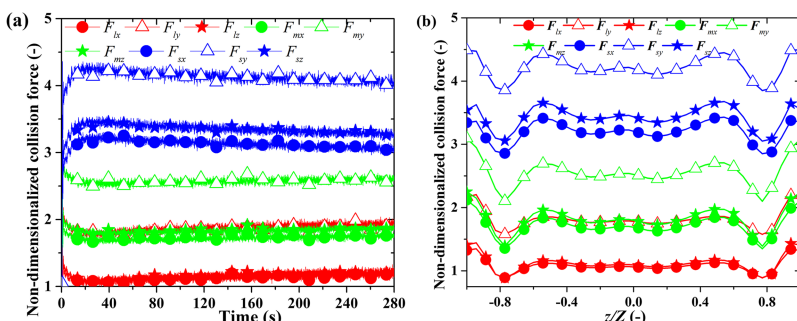


FIG. 8. Profiles of the non-dimensionalized collision force exerted on the three particle types (red, green, and blue represent large, medium, and small particles, respectively) in the rotating drum: (a) evolution of the instantaneous non-dimensionalized collision force with time and (b) time-averaged non-dimensionalized collision force along the drum length ( $z$ ).

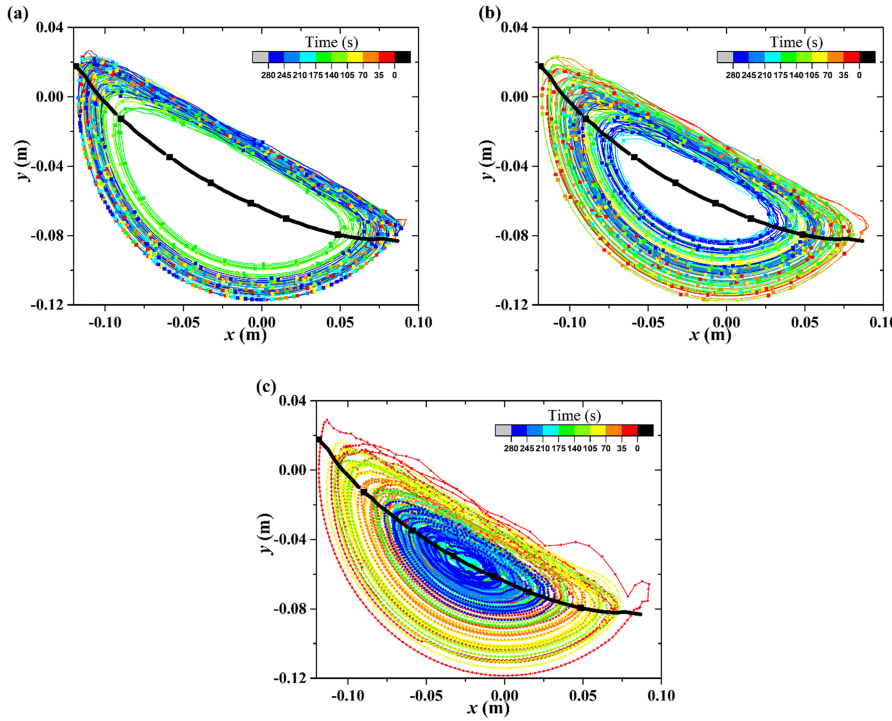


FIG. 9. Typical trajectory of the three particle types within the entire simulation duration: (a) large particle; (b) medium particle; and (c) small particle. Each black line represents the active-passive interface.

via DEM, the sample size is extremely large and statistically reliable.

#### F. Solid residence time (SRT)

Because of the very different characteristics of the active and passive regions in the rotating drum, the duration that a particle spends in each region directly dictates the extent of heat and mass transfer and thereby the extent of treatment (e.g., reaction and drying). For example, in the coating process,

the exposure of the granular material in the active region has a strong effect on the coating efficiency and also the uniformity of the coating. Therefore, the residence time of the particles in both the active and passive regions is an important parameter that significantly influences the overall system performance but is challenging to characterize and predict.<sup>52</sup> By means of theoretical analysis and experiments, several empirical correlations have been proposed to predict the solid residence time (SRT) in the rotating drum.<sup>42,51</sup> However, these correlations are generally proposed for the whole system. In view of the

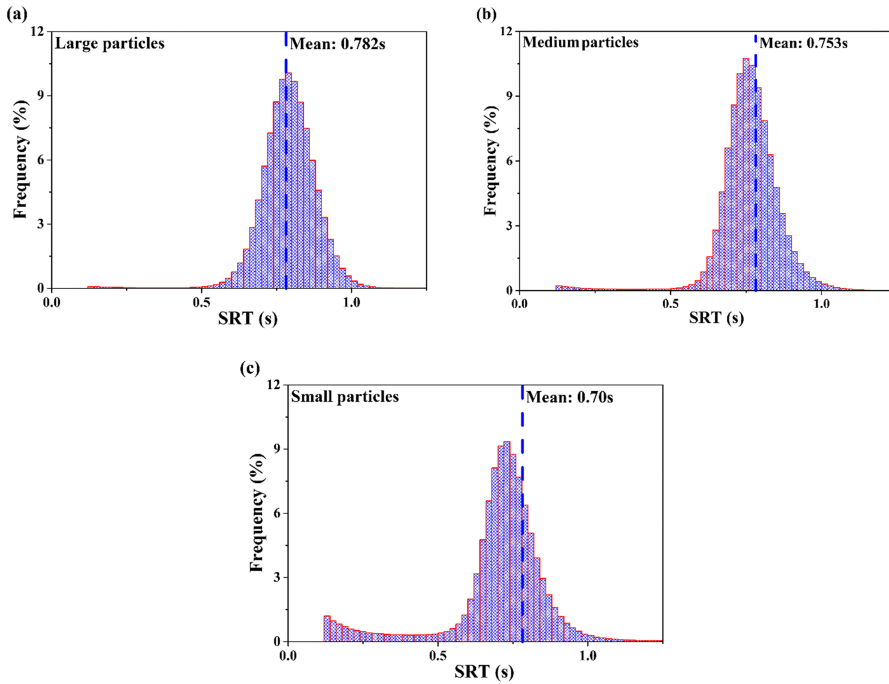


FIG. 10. Probability histogram of the solid residence time (SRT) of each particle type in the active region over the entire simulation duration, where each blue line stands for the mean SRT: (a) large particles; (b) medium particles; and (c) small particles.

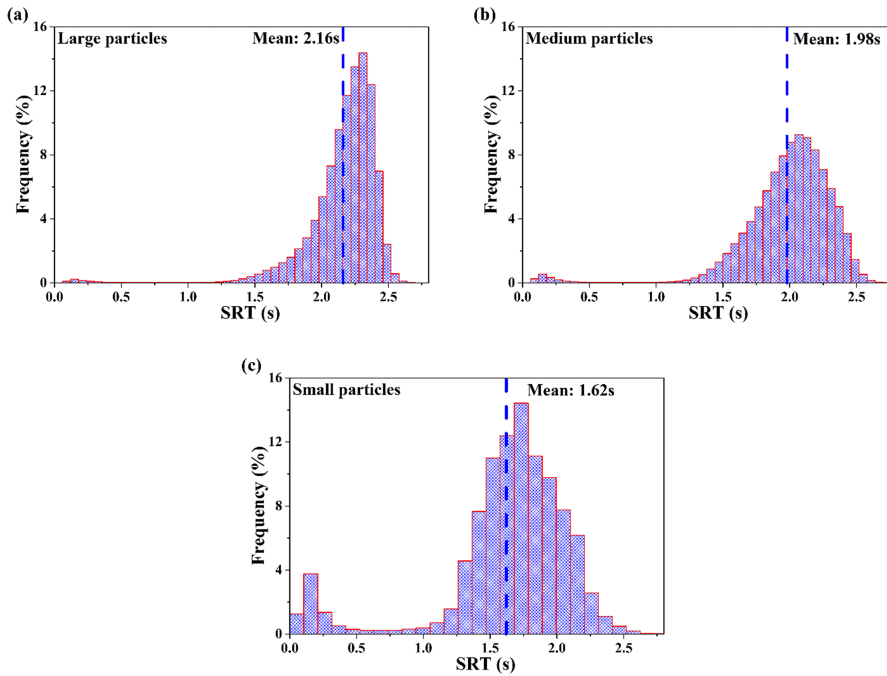


FIG. 11. Probability histogram of the solid residence time for each particle type in the passive region over the entire simulation duration, where each blue line stands for the mean SRT: (a) large particles; (b) medium particles; and (c) small particles.

marked differences in behavior between the active and passive regions, the more in-depth inspection of the SRT of each particle type in each of the two regions in this study would not only enhance the accuracy of such predictions but also shed new insights on the segregation phenomenon.

To evaluate the solid residence time (SRT) in each region, a counter is assigned to every particle in the system to track the time elapsed. Specifically, when a particle crosses the active-passive boundary, the counter is zeroed and starts to record the time the particle stays in this region until the active-passive boundary is crossed again. Figure 10 illustrates the probability histogram of the SRT of each particle type in the active region of the rotating drum, where each blue line represents the mean. General trends are described as follows: (i) the SRT distributions of all three particle types in the active region are approximately normal distributions with mean values approximately corresponding to the peak values, which is mainly due to the cyclic, regular motion of the particles (Fig. 9); (ii) at the lower SRT values ( $<0.5$  s), the probability is negligible for the large particles but not for the small particles because of the respective congregation in the radial periphery and core [Figs. 9(a) and 9(c)]; (iii) the mean SRT of the large particles is greatest, followed by medium and then small because the congregation of the larger particles in the radial periphery implies greatest displacements [Fig. 9(a)]. Compared to the binary-size mixture,<sup>53</sup> the presence of the additional medium particles does not qualitatively change the distribution of the SRT values, but the quantitative impact is that the mean SRT of the small particles becomes a little higher due to the increased congregation to the radial core.

For the passive region, the SRT probability histogram of each particle type is illustrated in Fig. 11. Similar to that in the active region (Fig. 10), (i) the SRT distributions are dissimilar among the three particle types, (ii) the mean SRT of the large particles is the greatest, followed by the medium and then

small due to the preferential radial segregation (Fig. 9), and (iii) the small particles exhibit the greatest probability of SRT values  $<1.0$  s, followed by the medium and then large particles, due to the congregation of the small particles in the radial core. In contrast to that in the active region (Fig. 10), (i) the SRT distributions are not normal, particularly with the SRT distribution of the large particles such that the peak is skewed the most rightward; and (ii) the mean SRT values for each particle type in the passive region are two to three times that in the active region. Compared to that of binary-size mixture,<sup>53</sup> the presence of the third particle type does not change the SRT probability distribution of both the large and small particles in the passive region. Collectively, these highlight the importance of considering region (i.e., active and passive) and particle size in characterizing SRT.

## G. Exchange rates between active and passive regions

The particles continuously traverse between the active and passive regions through the active-passive interface, and such exchanges critically influence the performance and efficiency of the rotating drum. The mass flow rates of each particle type and all the particles between the active and passive regions are quantified with respect to time in Fig. 12. Steep changes in the exchange rates occur within the first 40 s due to radial segregation, after which the changes due to the slow axial segregation are gradual. More specifically, the radial segregation causes the exchange rates of the large and medium particles to decrease, while that of the small particles to increase because of the preferential segregation of the large and small particles, respectively, to the radial periphery and core. Then the axial segregation causes the opposite trends, as in the exchange rates of the large and medium particles to increase, while that of the small particles to decrease because the formation of the axial bands consisting mostly of one particle type enhances and diminishes the exchanges, respectively, of the large and

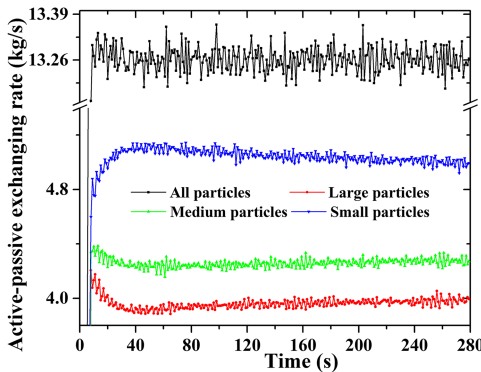


FIG. 12. Evolution of the solid exchange rates of the three particle types between the active and passive regions through the active-passive interface.

small particles. The greatest exchange rates of the small particles are tied to the lowest SRT values [Figs. 10(b) and 11(b)], and vice versa for the large particles. Notably the exchange rate of the medium particles is in between that of the large and small and mimics the large particles more although with more gentle changes with respect to time.

#### H. Axial dispersion behavior

The axial ( $z$ -directional) dispersion of the particles is an important characteristic in the rotating drum that warrants more understanding, since it underlies axial segregation. Previous efforts have shed some light,<sup>54</sup> and this study aims to advance the understanding through the Lagrangian perspective by means of Einstein's equation.<sup>55</sup> Figure 13 presents the contour plots of the spatially resolved distribution of the axial

dispersion coefficients of the large, medium, and small particle types in the central slice  $z/Z = 0$  of the rotating drum, where each black line stands for the active-passive interface. The local axial dispersion of each particle type is evaluated by averaging the dispersion coefficients of all the particles of this type throughout the entire simulation duration. In general, it is clear that the axial dispersion coefficients in the active region are greater than that in the passive due to the greater axial velocities (Table III), and the greatest dispersions for three particle types lie near the particle bed surface, which is in accordance with the collision force trends along this direction (Fig. 7).

To evaluate the dynamical response of the axial dispersion of the different particle types to the segregation phenomenon in the rotating drum, Fig. 14(a) displays the evolution of the axial dispersion coefficients ( $D_z$ ) in the rotating drum over the entire simulation duration. Similar to previous trends with respect to time, the radial segregation gives rise to sharper changes within the first 40 s and then the slower axial segregation causes slower changes subsequently. The axial dispersion coefficients ( $D_z$ ) are the greatest for the large particles, followed by the medium and then small ones. This is tied to the radial segregation of the large particles to the radial periphery and thereby the active region.

The axial segregation has been shown to change the axial distributions of the velocity (Fig. 6) and collision force (Fig. 8) of the different particle types. Analogously, Fig. 14(b) illustrates the axial distribution profile of the time-averaged axial dispersion coefficients ( $D_z$ ) of the three particle types. Similarly, the axial dispersion coefficients ( $D_z$ ) are non-uniform axially along the drum length. The axial dispersion intensities of all three particle types are the greatest near the end walls and

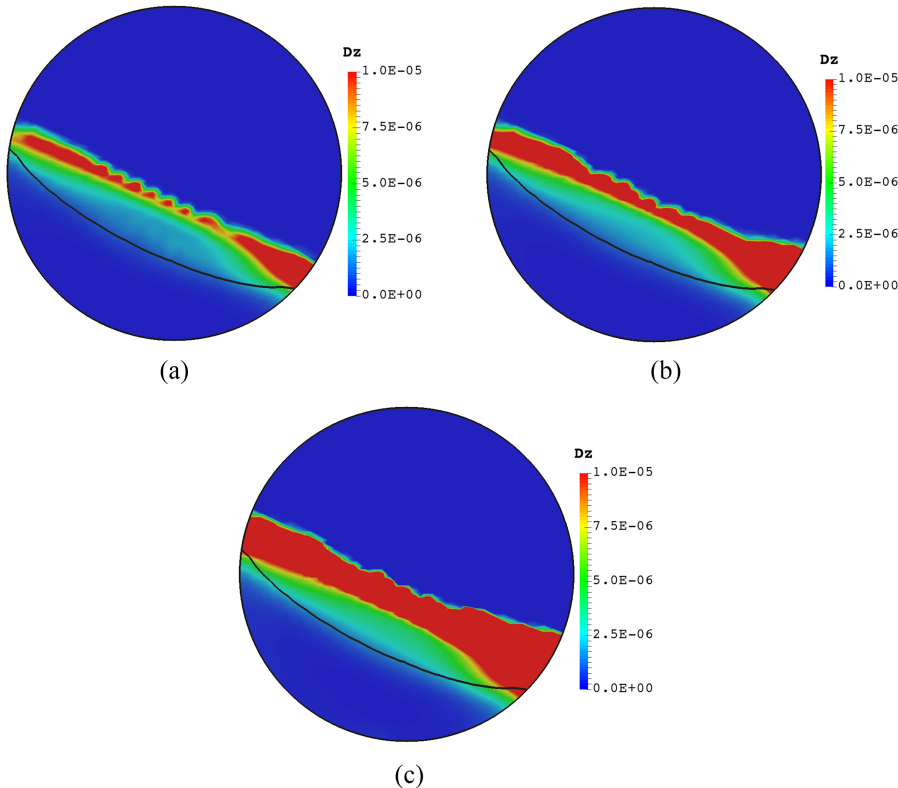


FIG. 13. Contour plots of the spatially resolved distribution of the axial dispersion coefficients in the central slice  $z/Z = 0$  of the rotating drum, where each black line stands for the active-passive interface: (a) large particles; (b) medium particles; and (c) small particles.

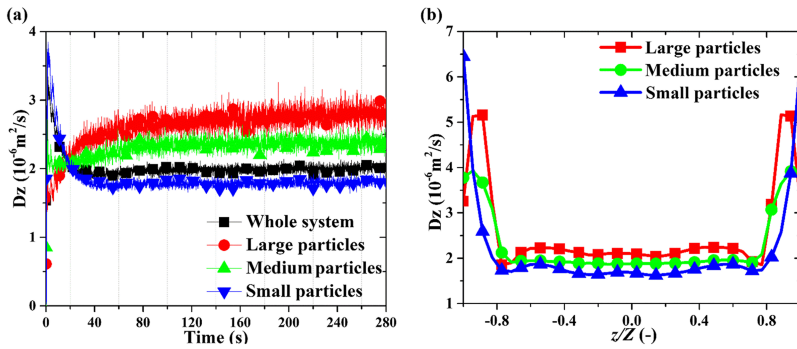


FIG. 14. (a) Evolution of the instantaneous axial dispersion coefficient for the different particle types over the entire simulation duration and (b) axial distribution profile of the time-averaged axial dispersion coefficient of the different particle types along the drum length.

comparatively much lower away from the end walls. Among the three particle types, the  $D_z$  values of the large particles are the weakest at the end walls due to the axial band consisting mostly of large particles and greatest away from the end walls due to the radial segregation tendencies. Compared with the binary-size mixture,<sup>56</sup> the presence of medium particle type does not obviously change the distribution pattern and also the dispersion intensity of both particle types.

## V. CONCLUSIONS

The size-induced segregation characteristics of the ternary-size mixture (i.e., three different particle sizes) in the rotating drum operating in the rolling mode is numerically investigated by means of the discrete element method (DEM) in the Lagrangian framework. Based on the results, the following conclusions can be drawn:

- (1) The size difference of the particles of the ternary-size mixture gives rise to the fast appearance of radial segregation followed by the slow axial segregation, which is similar to that of the binary-size mixture. Specifically, along the transverse ( $x$ - $y$ ) plane, the small particles congregate in the radial core, the large particles congregate in the radial periphery, while the medium particles are sandwiched in between. Along the axial direction, the radial core of small particles nearly spans the whole drum length, except at the end walls whereby axial bands consisting mostly of the large particles exist. The radial and axial segregation tendencies of the large and small particles are similar to that in a binary-size mixture, and the presence of the medium particles in the ternary-size mixture is such that they are sandwiched between the other two particle types in both the transverse and axial directions.
- (2) Similar to the systems with the monodisperse and binary-size mixture, the active-passive interface can be identified with positions of zero streamwise velocity and has similar heights throughout most of the drum length except near the end walls.
- (3) The radial and axial segregation of the ternary-size mixture changes the translational ( $U$ ) and rotational ( $\omega$ ) velocities of the different particle types. Sharper changes with respect to time are exhibited by the large and small particles, while more gentle changes are associated with the medium particles. The greatest velocity magnitudes are observed for the large particles, followed by the
- (4) The collision force is expectedly greater in the active region especially near the bed surface. The radial and axial segregation leads to the variation and also the non-uniform axial distribution of the collision forces exerted on the three particle types in the rotating drum. In general, the small and large particles experience, respectively, the greatest and least non-dimensionalized collision force along all three directions, which is similar to that in the binary-size mixture. The effect of the third particle type in the ternary-size mixture is such that the collision forces on the large and small particles are, respectively, decreased and increased in both regions.
- (5) The segregation phenomenon leads to the greatest and least SRT, respectively, for the large and small particles in both the active and passive regions. While the SRT frequency distributions of all three particle types are approximately normal in the active region, they are not so in the passive region, and the mean SRT values in the passive region are about two or three times of that in the active region. Compared to the binary-size mixture, the presence of the additional medium particles does not qualitatively change the distribution of the SRT values, but the quantitative impact is that the mean SRT of the small particles becomes lower due to the increased congregation to the radial core.
- (6) Radial segregation causes the exchange rates of the large and medium particles to decrease, while that of the small particles to increase, and then axial segregation causes the exchange rates of the large and medium particles to increase, while that of the small particles to decrease. The presence of the medium particle type expectedly diminishes the rates of both the large and small particles due to the reduced total mass of these two particle types. Interestingly, the ratio of the exchange rate of the small to large particles increases from 1.21 for the binary-size to 1.26 for the ternary-size, due to the enhanced extent of radial segregation in the latter case.

medium and then the small ones because of the preferential radial segregation of the large and small particles, respectively, to the periphery and core, and the medium ones in between. The presence of the third particle type in the ternary-size mixture exerts a negligible influence on the velocities of the large particles in both the regions but clearly decreases the translational velocity of the small particles in the transverse plane.

- (7) The spatially resolved axial dispersion intensities of all three particle types are the greatest in the active region especially near the bed surface. The large and small particles exhibit the greatest and lowest dispersion intensities throughout most of the drum length, and the medium particles have intermediate values. The presence of the medium particle type does not obviously alter the dispersion pattern and intensity for large and small particle types.

The findings from the current work shed insights with respect to segregation on the effect of an additional particle type on the binary-size mixture, which has been popularly studied. Two further knowledge gaps that warrant future studies are noted. First, a complete understanding of the intrinsic mechanism underlying axial segregation remains elusive, despite the axial segregation phenomenon being observed nearly 70 years ago. The inextricable role of friction induced by the end walls suggests that a detailed analysis of particle-particle and particle-wall friction forces generated upon collision would be useful for deciphering the genesis of axial segregation near the end walls and the band travelling phenomenon. Second, although continuous particle size distributions are prevalent both in natural and industrial processes, little is known on the effect of multiple particle sizes on granular segregation, at least in part because of the significantly higher computational expense. The non-negligible impact of an additional particle type on a binary-size mixture suggests that further unraveling of the effect of multiple particle types would be valuable.

## ACKNOWLEDGMENTS

The authors thank the financial support from the National Research Foundation (NRF), Prime Minister's Office, Singapore under its Campus for Research Excellence and Technological Enterprise (CREATE) program.

- <sup>1</sup>Y. Forterre and O. Pouliquen, "Flows of dense granular media," *Annu. Rev. Fluid Mech.* **40**, 1–24 (2008).
- <sup>2</sup>A. Bhatjea, I. Sharma, and J. K. Singh, "Scaling of granular temperature in vibro-fluidized grains," *Phys. Fluids* **28**, 043301 (2016).
- <sup>3</sup>G. Saingier, S. Deboeuf, and P. Y. Lagrée, "On the front shape of an inertial granular flow down a rough incline," *Phys. Fluids* **28**, 053302 (2016).
- <sup>4</sup>T. C. Kumawat and N. Tiwari, "Stability analysis of the rimming flow inside a uniformly heated rotating horizontal cylinder," *Phys. Fluids* **29**, 032102 (2017).
- <sup>5</sup>P. Y. Liu, R. Y. Yang, and A. B. Yu, "Dynamics of wet particles in rotating drums: Effect of liquid surface tension," *Phys. Fluids* **23**, 013304 (2011).
- <sup>6</sup>J. M. N. T. Gray, "Granular flow in partially filled slowly rotating drums," *J. Fluid Mech.* **441**, 1–29 (2001).
- <sup>7</sup>J. Mellmann, "The transverse motion of solids in rotating cylinders—Forms of motion and transition behavior," *Powder Technol.* **118**, 251–270 (2001).
- <sup>8</sup>J. M. Ottino and D. V. Khakhar, "Mixing and segregation of granular materials," *Annu. Rev. Fluid Mech.* **32**, 55–91 (2000).
- <sup>9</sup>S. R. Dahl and C. M. Hrenya, "Size segregation in rapid, granular flows with continuous size distributions," *Phys. Fluids* **16**, 1–13 (2004).
- <sup>10</sup>S. Das Gupta, D. V. Khakhar, and S. K. Bhatia, "Axial segregation of particles in a horizontal rotating cylinder," *Chem. Eng. Sci.* **46**, 1513–1517 (1991).
- <sup>11</sup>C. M. Dury and G. H. Ristow, "Competition of mixing and segregation in rotating cylinders," *Phys. Fluids* **11**, 1387–1394 (1999).
- <sup>12</sup>I. Zuriguel, J. Peixinho, and T. Mullin, "Segregation pattern competition in a thin rotating drum," *Phys. Rev. E* **79**, 051303 (2009).
- <sup>13</sup>I. Zuriguel, J. M. N. T. Gray, J. Peixinho, and T. Mullin, "Pattern selection by a granular wave in a rotating drum," *Phys. Rev. E* **73**, 061302 (2006).
- <sup>14</sup>Z. S. Khan, F. Van Bussel, M. Schaber, R. Seemann, M. Scheel, and M. Di Michiel, "High-speed measurement of axial grain transport in a rotating drum," *New J. Phys.* **13**, 105005 (2011).
- <sup>15</sup>A. N. Huang and H. P. Kuo, "A study of the three-dimensional particle size segregation structure in a rotating drum," *AIChE J.* **58**, 1076–1083 (2012).
- <sup>16</sup>G. Juarez, J. M. Ottino, and R. M. Lueptow, "Axial band scaling for bidisperse mixtures in granular tumblers," *Phys. Rev. E* **78**, 031306 (2008).
- <sup>17</sup>C. Windows-Yule, B. J. Scheper, A. J. van der Horn, N. Hainsworth, J. Saunders, D. J. Parker, and A. R. Thornton, "Understanding and exploiting competing segregation mechanisms in horizontally rotated granular media," *New J. Phys.* **18**, 023013 (2016).
- <sup>18</sup>S. Inagaki, H. Ebata, and K. Yoshikawa, "Steadily oscillating axial bands of binary granules in a nearly filled coaxial cylinder," *Phys. Rev. E* **91**, 010201 (2015).
- <sup>19</sup>F. A. M. S. Tilo, "The mechanism of long-term coarsening of granular mixtures in rotating drums," *New J. Phys.* **17**, 093023 (2015).
- <sup>20</sup>R. Y. Yang, R. P. Zou, and A. B. Yu, "Numerical study of the packing of wet coarse uniform spheres," *AIChE J.* **49**, 1656–1666 (2003).
- <sup>21</sup>N. Gui, X. Yang, S. Jiang, J. Tu, and J. Fan, "Extended HPM-DEM coupled simulation of drainage of square particles in a 2D hopper flow," *AIChE J.* **62**, 1863–1876 (2016).
- <sup>22</sup>S. Mandal and D. V. Khakhar, "A study of the rheology of planar granular flow of dumbbells using discrete element method simulations," *Phys. Fluids* **28**, 103301 (2016).
- <sup>23</sup>C. Kuo, L. Sheng, S. Chiu, Y. Yang, Y. Tai, and S. Hsiao, "Measurement and discrete element simulation of a fixed-obstacle disturbed rapid granular chute flow," *Phys. Fluids* **27**, 013305 (2015).
- <sup>24</sup>P. Richard and N. Taberlet, "Recent advances in DEM simulations of grains in a rotating drum," *Soft Matter* **4**, 1345–1348 (2008).
- <sup>25</sup>R. Y. Yang, A. B. Yu, L. McElroy, and J. Bao, "Numerical simulation of particle dynamics in different flow regimes in a rotating drum," *Powder Technol.* **188**, 170–177 (2008).
- <sup>26</sup>D. C. Rapaport, "Simulational studies of axial granular segregation in a rotating cylinder," *Phys. Rev. E* **65**, 061306 (2002).
- <sup>27</sup>G. J. Finnie, N. P. Krut, M. Ye, C. Zeilstra, and J. A. M. Kuipers, "Longitudinal and transverse mixing in rotary kilns: A discrete element method approach," *Chem. Eng. Sci.* **60**, 4083–4091 (2005).
- <sup>28</sup>N. Taberlet and P. Richard, "Diffusion of a granular pulse in a rotating drum," *Phys. Rev. E* **73**, 041301 (2006).
- <sup>29</sup>D. C. Rapaport, "Radial and axial segregation of granular matter in a rotating cylinder: A simulation study," *Phys. Rev. E* **75**, 031301 (2007).
- <sup>30</sup>P. Chen, J. M. Ottino, and R. M. Lueptow, "Subsurface granular flow in rotating tumblers: A detailed computational study," *Phys. Rev. E* **78**, 021303 (2008).
- <sup>31</sup>P. Chen, J. M. Ottino, and R. M. Lueptow, "Onset mechanism for granular axial band formation in rotating tumblers," *Phys. Rev. Lett.* **104**, 188002 (2010).
- <sup>32</sup>S. Yang, Y. Sun, L. Zhang, and J. W. Chew, "Segregation dynamics of a binary-size mixture in a three-dimensional rotating drum," *Chem. Eng. Sci.* **172**, 652–666 (2017).
- <sup>33</sup>Y. Yu and H. Saxén, "Experimental and DEM study of segregation of ternary size particles in a blast furnace top bunker model," *Chem. Eng. Sci.* **65**, 5237–5250 (2010).
- <sup>34</sup>M. Newey and J. Ozik, "Band-in-band segregation of multidisperse granular mixtures," *Europhys. Lett.* **66**, 205 (2004).
- <sup>35</sup>H. A. Makse, S. Havlin, P. R. King, and H. E. Stanley, "Spontaneous stratification in granular mixtures," *Nature* **386**, 379–382 (1997).
- <sup>36</sup>M. Shimokawa, Y. Suetsugu, R. Hiroshige, T. Hirano, and H. Sakaguchi, "Pattern formation in a sandpile of ternary granular mixtures," *Phys. Rev. E* **91**, 062205 (2015).
- <sup>37</sup>T. Akiyama, K. Yamamoto, and S. Okutsu, "A solid-solid extraction," *Powder Technol.* **110**, 190–195 (2000).
- <sup>38</sup>S. K. Hajra and D. V. Khakhar, "Radial segregation of ternary granular mixtures in rotating cylinders," *Granular Matter* **13**, 475–486 (2011).
- <sup>39</sup>D. C. Rapaport, "Simulated three-component granular segregation in a rotating drum," *Phys. Rev. E* **76**, 041302 (2007).
- <sup>40</sup>G. G. Pereira and P. W. Cleary, "Radial segregation of multi-component granular media in a rotating tumbler," *Granular Matter* **15**, 705–724 (2013).
- <sup>41</sup>E. Alizadeh, O. Dubé, F. Bertrand, and J. Chaouki, "Characterization of mixing and size segregation in a rotating drum by a particle tracking method," *AIChE J.* **59**, 1894–1905 (2013).

- <sup>42</sup>E. Alizadeh, F. Bertrand, and J. Chaouki, "Comparison of DEM results and Lagrangian experimental data for the flow and mixing of granules in a rotating drum," *AIChE J.* **60**, 60–75 (2014).
- <sup>43</sup>P. A. Cundall and O. D. L. Strack, "A discrete numerical model for granular assemblies," *Geotechnique* **29**, 47–65 (1979).
- <sup>44</sup>J. Ai, J. Chen, J. M. Rotter, and J. Y. Ooi, "Assessment of rolling resistance models in discrete element simulations," *Powder Technol.* **206**, 269–282 (2011).
- <sup>45</sup>C. Goniva, C. Kloss, N. G. Deen, J. A. M. Kuipers, and S. Pirker, "Influence of rolling friction on single spout fluidized bed simulation," *Particuology* **10**, 582–591 (2012).
- <sup>46</sup>S. Yang, K. Luo, J. Fan, and K. Cen, "Particle-scale investigation of the solid dispersion and residence properties in a 3-D spout-fluid bed," *AIChEJ.* **60**, 2788–2804 (2014).
- <sup>47</sup>S. Yang, A. Cahyadi, J. Wang, and J. W. Chew, "DEM study of granular flow characteristics in the active and passive regions of a three-dimensional rotating drum," *AIChE J.* **62**, 3874–3888 (2016).
- <sup>48</sup>J. M. N. T. Gray and C. Ancey, "Multi-component particle-size segregation in shallow granular avalanches," *J. Fluid Mech.* **678**, 535–588 (2011).
- <sup>49</sup>K. M. Hill and J. Kakalios, "Reversible axial segregation of rotating granular media," *Phys. Rev. E* **52**, 4393–4400 (1995).
- <sup>50</sup>M. Rasouli, O. Dubé, F. Bertrand, and J. Chaouki, "Investigating the dynamics of cylindrical particles in a rotating drum using multiple radioactive particle tracking," *AIChE J.* **62**, 2622–2634 (2016).
- <sup>51</sup>Y. L. Ding, R. Forster, J. P. K. Seville, and D. J. Parker, "Granular motion in rotating drums: Bed turnover time and slumping–rolling transition," *Powder Technol.* **124**, 18–27 (2002).
- <sup>52</sup>I. J. Paredes, B. Yohannes, H. Emady, B. J. Glasser, W. G. Borghard, F. Muzzio, A. M. Cuitiño, J. Beeckman, S. Ilias, P. Podsiadlo, E. Jezek, and J. Baumgartner, "The effect of operating conditions on the residence time distribution and axial dispersion coefficient of a cohesive powder in a rotary kiln," *Chem. Eng. Sci.* **158**, 50–57 (2017).
- <sup>53</sup>S. Yang, Y. Sun, L. Zhang, and J. W. Chew, "Impact of granular segregation on the solid residence time and active–passive exchange in a rotating drum," *Chem. Eng. Sci.* **173**, 287–302 (2017).
- <sup>54</sup>I. C. Christov and H. A. Stone, "Resolving a paradox of anomalous scalings in the diffusion of granular materials," *Proc. Natl. Acad. Sci. U. S. A.* **109**, 16012–16017 (2012).
- <sup>55</sup>A. Einstein, *Investigations on the Theory of the Brownian Movement* (Courier Dover Publications, 1956).
- <sup>56</sup>S. Yang, L. Zhang, K. Luo, and J. W. Chew, "DEM investigation of the axial dispersion behavior of a binary-size granular mixture in the horizontal rotating drum," *Powder Technol.* (submitted).